Article

Structure

The Structure of a BamA-BamD Fusion Illuminates the Architecture of the β-Barrel Assembly Machine Core

Graphical Abstract

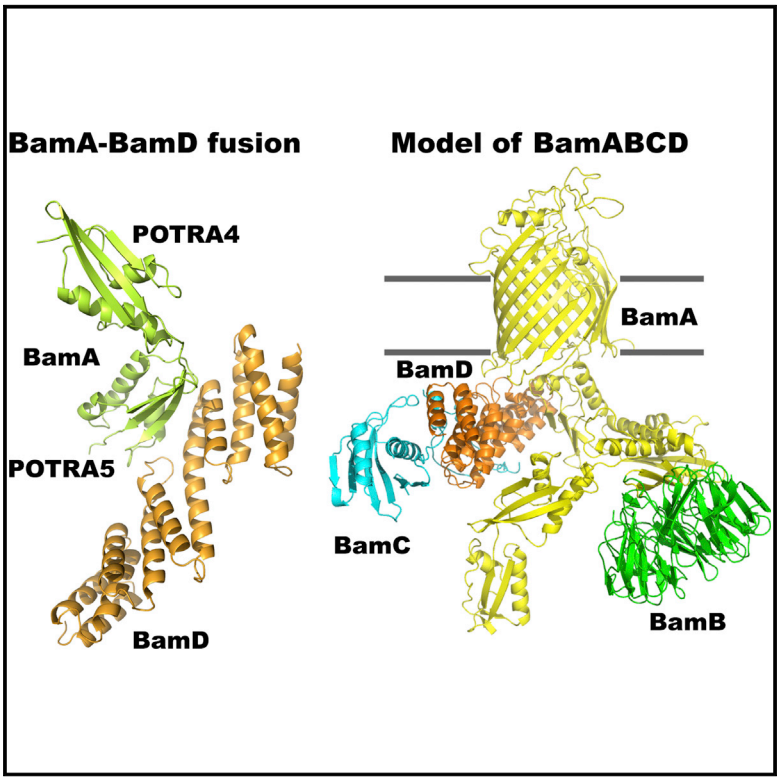

Authors

Hans Thor Bergal, Alex Hunt Hopkins, Sandra Ines Metzner, Marcelo Carlos Sousa

Correspondence

marcelo.sousa@colorado.edu

In Brief

Insertion and folding of β-barrel proteins into the bacterial outer membrane is carried out by the β-barrel assembly machine (BAM) complex. Bergal et al. elucidate the crystal structure of a BamA-BamD fusion and present a model of the BamABCD core complex.

Highlights

- BamA POTRA5 binds BamD in a groove formed by TPR4 and the loop of TPR3
- The observed interface is validated by mutagenesis and disulfide crosslinking
- The structure allows the construction of a near-complete BAM complex model
- A membrane-adjacent periplasmic ring in BAM is proposed to bind nascent OMPs

Accession Numbers

5EFR

Bergal et al., 2016, Structure *24*, 243–251
February 2, 2016
http://dx.doi.org/10.1016/j.str.2015.10.030

Structure
Article

The Structure of a BamA-BamD Fusion Illuminates the Architecture of the β-Barrel Assembly Machine Core

Hans Thor Bergal,[1] Alex Hunt Hopkins,[1] Sandra Ines Metzner,[1] and Marcelo Carlos Sousa[1,*]
[1]Department of Chemistry and Biochemistry, University of Colorado at Boulder, Boulder, CO 80309, USA
*Correspondence: marcelo.sousa@colorado.edu
http://dx.doi.org/10.1016/j.str.2015.10.030

SUMMARY

The β-barrel assembly machine (BAM) mediates folding and insertion of integral β-barrel outer membrane proteins (OMPs) in Gram-negative bacteria. Of the five BAM subunits, only BamA and BamD are essential for cell viability. Here we present the crystal structure of a fusion between BamA POTRA4-5 and BamD from *Rhodothermus marinus*. The POTRA5 domain binds BamD between its tetratricopeptide repeats 3 and 4. The interface structural elements are conserved in the *Escherichia coli* proteins, which allowed structure validation by mutagenesis and disulfide crosslinking in *E. coli*. Furthermore, the interface is consistent with previously reported mutations that impair BamA-BamD binding. The structure serves as a linchpin to generate a BAM model where POTRA domains and BamD form an elongated periplasmic ring adjacent to the membrane with a central cavity approximately 30 × 60 Å wide. We propose that nascent OMPs bind this periplasmic ring prior to insertion and folding by BAM.

INTRODUCTION

Proteins integral to the outer membrane of diderm bacteria are characterized by the β-barrel structure of their transmembrane domain. In contrast to α-helical proteins of the inner membrane whose membrane insertion is co-translational, folding and insertion of β-barrel outer membrane proteins (OMPs) are post-translational. They require translocation across the inner membrane, transport across the aqueous periplasmic space, and specific delivery to the outer membrane where they must insert and fold. In the current consensus model for this essential process, newly synthesized OMPs are post-translationally translocated across the inner membrane by the SecYEG translocon in a SecA-dependent manner. Once in the periplasm, they are thought to be captured by periplasmic chaperones that prevent their aggregation. Both SurA and Skp have been implicated in the OMP biogenesis pathway (Lyu and Zhao, 2015). Although they may have overlapping functions, SurA plays a more prevalent role in *Escherichia coli* (Sklar et al., 2007b) while Skp appears to be more important in *Neisseria* (Volokhina et al., 2011). The outer membrane-embedded multiprotein complex known as the β-barrel assembly machine (BAM) then mediates folding and insertion of β-barrel OMPs into the outer membrane (Sklar et al., 2007a; Wu et al., 2005).

The central component of BAM is BamA, itself a β-barrel OMP with a large periplasmic domain. BamA is present in all diderm bacteria (Heinz and Lithgow, 2014; Sutcliffe, 2010) and is essential for cell viability (Bos et al., 2004; Ruiz et al., 2005; Voulhoux and Tommassen, 2004; Wu et al., 2005). Homologs of BamA are also present in eukaryotic mitochondria and chloroplasts where they play a fundamental role in β-barrel folding and insertion (Gentle et al., 2004; Hsu and Inoue, 2009). In *E. coli*, the BAM complex contains four additional subunits, the lipoproteins BamBCDE (Sklar et al., 2007a; Wu et al., 2005). The individual deletion of the *bamB*, *bamC*, or *bamE* genes has relatively mild phenotypes in *E. coli*, resulting in membrane permeability defects that render the bacteria more sensitive to antibiotics and other toxic compounds. Conversely, deletion of the *bamD* gene is lethal. This functional hierarchy of the lipoproteins is consistent with their phylogenetic distribution. Like BamA, BamD is present in every diderm bacteria, whereas the other lipoproteins are not, suggesting that BamD has an important role in BAM function. Whereas the molecular mechanism of OMP folding and insertion remains unclear, BamA has been proposed to bind nascent OMPs by β-augmentation (Gatzeva-Topalova et al., 2008; Kim et al., 2007) and facilitate their assembly. However, it was recently reported that BamD may also interact directly with substrate OMPs by recognizing a consensus sequence, and mutation of this sequence in the substrate impairs its folding and insertion (Hagan et al., 2015). Together, these data suggest that BamA-BamD constitute the fundamental functional core of BAM.

The structures of all the individual BAM subunits have been reported (Albrecht and Zeth, 2011; Endo et al., 2011; Heuck et al., 2011; Jansen et al., 2012; Kim and Paetzel, 2011; Knowles et al., 2011; Noinaj et al., 2011, 2013; Sandoval et al., 2011; Warner et al., 2011). BamA is a β-barrel OMP with an N-terminal periplasmic domain composed of five polypeptide translocation associated (POTRA) motifs. BamBCDE are otherwise soluble proteins that are anchored to the outer membrane by lipids attached to their N-terminal cysteine. Most of the subunit interactions are thus thought to occur between the periplasmic components of the complex. Genetic and biochemical data suggest that BamAB and BamCDE form two separable subcomplexes that come together to form the whole complex through interactions between BamA and BamD (Hagan et al., 2010; Kim et al.,

Table 1. Data Collection and Refinement Statistics

Data Collection	BamA:BamD
Wavelength (Å)	1.000
Resolution (Å)[a]	30.00–2.00 (2.03–2.00)
Space group	$P2_1$
Cell dimensions (Å)	a = 69.9, b = 48.1, c = 78.0, β = 104.3°
Unique reflections	33,843 (1,659)
Completeness (%)	98.4 (99.1)
Average redundancy	3.4 (3.5)
I/σ	28.4 (1.9)
$R_{p.i.m.}$[b] (%)	4.4 (41.4)
Wilson B-factor	34.6
Refinement	
Resolution (Å)[a]	30.00–2.00 (2.06–2.00)
Reflections used in refinement	33,817 (3,165)
Reflections in test set	1,803 (169)
R_{work}[c] (%)	21.1 (30.7)
R_{free}[c] (%)	23.2 (37.1)
Number of non-hydrogen atoms	3,561
Number of amino acid residues	403
Mean B-value amino acids (Å^2)	46.1
Number of water molecules	208
Mean B-value waters (Å^2)	47.1
RMSD from ideal values	
Bond lengths (Å)	0.003
Bond angles (degrees)	0.6
Residues in Ramachandran plot	
Most favored regions (%)	97.7
Generously allowed regions (%)	2.3
Outliers (%)	0

[a]Values in parentheses are for the highest-resolution shell.
[b]$R_{p.i.m.} = \sum_{hkl}[1/(N-1)]^{1/2}\sum_i|I_i(hkl) - \langle I(hkl)\rangle|/\sum_{hkl}\sum_i I_i(hkl)$, where $I_i(hkl)$ is the Ith measurement of each reflection hkl, $\langle I(hkl)\rangle$ is the weighted mean of all measurements of hkl, and N is the number of unique reflections.
[c]$R_{work} = \sum|F_{obs} - F_{calc}|/\sum F_{obs}$, where F_{obs} = observed structure factor amplitude and F_{calc} = structure factor calculated from model. R_{free} is computed the same as R_{work}, but using the test set of reflections.

2007; Sklar et al., 2007a; Vuong et al., 2008; Wu et al., 2005). The crystal structures of BamD in complex with the N-terminal domains of BamC (Kim et al., 2011) and, more recently, that of BamB in complex with BamA POTRA34 (Jansen et al., 2015), have provided molecular detail of the subcomplexes. Here, we present the crystal structure of a fusion between BamD and the POTRA4-5 domains of BamA from the thermophilic bacterium *Rhodothermus marinus*. The structure reveals the interaction interface whose physiological relevance is validated by disulfide crosslinking and mutagenesis experiments in the full-length *E. coli* homologs. Residues in BamA and BamD previously shown to be important for their interaction also map to the interface, further validating the structure. Importantly, the structure serves as a linchpin that allows superposition of the high-resolution structures of individual subunits and known subcomplexes to provide a first glimpse of the BAM complex architecture.

RESULTS

Structure of a BamA-BamD Fusion

The N-terminal domain of BamA contains five POTRA domains with POTRA5 linked to the membrane-embedded C-terminal β-barrel. Previous genetic and biochemical data suggested that the interaction with BamD was mediated by POTRA5 (Kim et al., 2007; Ricci et al., 2012). BamD is composed of five tetratricopeptide repeats (TPRs) that, due to lipidation of its N-terminal cysteine, has its N-terminal TPR topologically close to the membrane (Albrecht and Zeth, 2011; Sandoval et al., 2011). It was then reasoned that linking the C terminus of POTRA5 to the N terminus of BamD with an appropriately long, flexible linker could result in a soluble fusion that allows formation of the native interface while dispensing with the membrane-embedded elements that may hinder crystallization. We recently utilized such a subunit fusion strategy to successfully define the interface between BamA and BamB (Jansen et al., 2015). Choosing an appropriate linker is crucial, as one that is too short would prevent formation of the native interface while an overly long one would likely interfere with crystallization. As BamD is approximately 90 Å long from the first TPR to the C terminus, a 22 amino acid linker was initially tested for the fusions. With a stretched length of more than 75 Å, it would accommodate most possible orientations between BamA and BamD while increasing the local concentrations of the proteins, helping stabilize a complex. The BamA periplasmic domain is known to be conformationally flexible due to a hinge between POTRA2 and POTRA3 (Gatzeva-Topalova et al., 2008, 2010). Therefore, to further increase the chances of crystallization, fusions containing only POTRA3-5 and POTRA4-5 were designed in addition to the full POTRA1-5 fragment. Screening of several constructs for expression and crystallization resulted in crystals of a fusion between POTRA4-5 (amino acids 303–467) and BamD (amino acids 24–280) from *R. marinus* linked by a 22-amino acid linker (sequence: HVASGGGGSGGGGSGGGG SGTS). Refinement of the crystallization conditions to 10% PEG-3000, 15% 2-propanol, and 0.1 M HEPES (pH 5.6) yielded single crystals suitable for X-ray diffraction analysis. A native dataset to 2.0-Å resolution was collected from cryoprotected crystals using synchrotron radiation. Data collection statistics are shown in Table 1.

The structure was determined by molecular replacement using *R. marinus* BamD (Sandoval et al., 2011) and *E. coli* POTRA4-5 (Gatzeva-Topalova et al., 2010) as search models. Several rounds and manual model rebuilding and refinement resulted in a model containing residues 303–467 of BamA encompassing all of POTRA4 and 5, and residues 30–266 of BamD containing all the TPR repeats and capping helices of BamD. As expected, no clear electron density was detected for the glycine/serine-rich flexible linker joining BamA and BamD. Refinement statistics for the final models are summarized in Table 1.

POTRA domains have a canonical β1-α1-α2-β2-β3 architecture where the three β strands form a mixed β-sheet that packs against the two α-helices (Gatzeva-Topalova et al., 2008; Kim et al., 2007). The crystal structure of the BamA-BamD fusion (Figure 1) shows that POTRA4 in *R. marinus* BamA (rmBamA) follows the canonical architecture while POTRA5 displays a variation

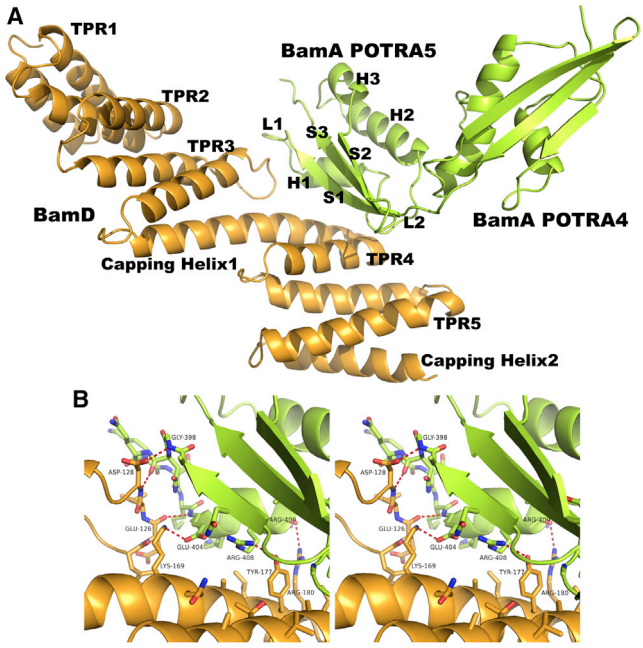

Figure 1. Structure of BamA(POTRA4-5)-BamD Fusion

(A) Overall cartoon representation of the crystallographic model of rmBamA(POTRA4-5) (lime) and rmBamD (light orange). Strand S1, loop (L1), helix1 (H1), and loop 2 (L2) of POTRA5 interface with TPR4 and the loop of TPR3 in BamD.

(B) Close-up stereo representation of the rmBamA-rmBamD interface. Relevant main-chain and side-chain residues are shown as sticks. Hydrogen bonds and a salt bridge are shown as red dashed lines.

where the beginning of strand 1 (S1) has an insert that folds into a short α-helix (H3) (Figure 1A). The first three TPRs of BamD form an N-terminal domain capped by an α-helix (capping helix 1), which extends to become the first helix of TPR4 (Figure 1A). This arrangement offsets the C-terminal TPRs 4 and 5 with respect to the N-terminal domain breaking the superhelical twist that is typical of TPR repeat proteins (Allan and Ratajczak, 2010) and giving BamD an elongated and flat structure (Sandoval et al., 2011). In *R. marinus* BamD (rmBamD), the C-terminal TPR5 is also capped by an α-helix (capping helix 2; Figure 1A) (Sandoval et al., 2011). The crystal structure of the BamA-BamD fusion reveals that TPR4 and the loop connecting the two helices of TPR3 in rmBamD interact primarily with strand 1 (S1), loop 1 (L1), helix 1 (H1), and loop 2 (L2) of the POTRA5 domain of rmBamA (Figures 1A and 1B). The interface was the largest in the crystal lattice and buries approximately 650 $Å^2$ of surface area as calculated using PDBePISA (Krissinel and Henrick, 2007). No interactions between BamD and POTRA4 of BamA were observed.

The helix-turn-helix motif of rmBamD TPR4 packs tightly against strand S1, helix H1, and loop L2 that connects helices 1 and 2 in POTRA5 (Figure 1). The side chains of rmBamD R180 and Y177 hydrogen bond to the main-chain carbonyl of R409 and the side-chain guanidinium of R408 of rmBamA, respectively (Figure 1B). The interface is further stabilized by several interactions between the L1 loop in rmBamA and the loop of rmBamD TPR3. These include several hydrogen bonds and a salt bridge between rmBamA E404 and rmBamD K169 as depicted in Figure 1B.

Validation of the BamA-BamD Interface

Whereas *R. marinus* BamA and BamD fragments were amenable to crystallization and structure determination, expression of the thermophilic full-length proteins for functional assays is very difficult. Therefore, models of the *E. coli* BamA-BamD interface were generated such that functional assays could take advantage of the well-established *E. coli* platform. Superposition of the *E. coli* BamA (ecBamA) POTRA4-5 onto rmBamA POTRA5 shows excellent agreement (root-mean-square deviation [RMSD] 0.93 Å over 56 Cα atoms) with conformational conservation of all the POTRA5 elements important for the interface (Figure 2A, lime and yellow). Whereas the angle between POTRA4 and POTRA5 is slightly different between the structures, it does not affect the BamA-BamD interface. Comparison of the available structures of *E. coli* BamD (ecBamD) either isolated (Albrecht and Zeth, 2011; Dong et al., 2012) or in complex with BamC (Kim et al., 2011) reveals flexibility of the long helix that connects the N-terminal TPRs1-3 and the C-terminal TPRs4-5 (Figure S1). This flexibility is also apparent comparing the structure of isolated rmBamD (Sandoval et al., 2011) and that presented here in complex with rmBamA (Figure S1). Therefore, ecBamD was divided into N- and C-terminal domains and superimposed onto rmBamD TPR1-3 and TPR4, respectively. As with BamA, the structural elements important for the interface were conformationally conserved (Figure 2A). However, TPR3 in ecBamD contains an insert between its two helices that elongates the connecting loop and makes it conformationally labile (see Discussion). There is also a slight difference in the relative orientations of TPR4 and 5 between ecBamD and rmBamD, and ecBamD lacks a C-terminal capping helix (capping helix 2 in Figure 1). However, these elements are remote to the interface (Figure 2A). The quality of the superpositions suggests that the structure of the interface is conserved between the *Rhodothermus* and *E. coli* BamA-BamD. To further improve the model, the RosettaCM protocol for high-resolution comparative modeling was implemented (Song et al., 2013). This resulted in the ecBamA-BamD interface depicted in Figure 2B.

It has previously been shown that an E373K mutation in ecBamA is lethal to the cells because it disrupts the BamA-BamD interaction (Ricci et al., 2012). The lethal phenotype could be rescued by an R197L mutation in ecBamD. The modeled interface displays a direct interaction between BamA E373 and BamD R197 within a pocket lined by positively charged residues including BamA R353, R350, and R366 (Figure 2B). This is consistent with the previously reported effect of an E373K mutation disrupting the BamA-BamD interface in *E. coli* (Ricci et al., 2012) as the positive charge of a lysine at position 373 would not interact favorably with R197 and the positively charged pocket. BamD R197L suppresses the lethal phenotype of BamA E373K while not restoring BamA-BamD binding to clearly detectable levels, which led to the proposal that this BamD mutation may activate BamD and bypass the requirement to form BAM holocomplex (Ricci et al., 2012). Whether this is the case, or the R197L mutation restores enough binding to BamA E373K to allow BAM function but the interaction is too weak to

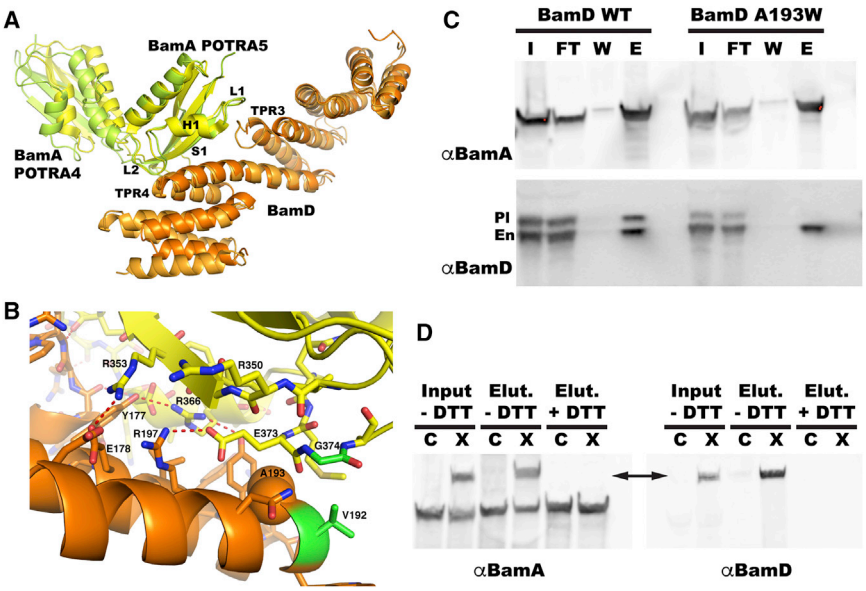

Figure 2. *E. coli* BamA(POTRA4-5)-BamD Model and Validation

(A) Superposition of rmBamA-BamD (lime and light orange, respectively) and ecBamA-BamD (yellow and bright orange) showing structural conservation of the interface.

(B) Close-up view of the ecBamA-BamD interface after RosettaCM minimization. BamA E373 and BamD R197 previously implicated in the BamA-BamD interface display a direct interaction. BamA residue A193 chosen for mutation to tryptophan to probe the interface is shown as a space-filling model. BamA G374 and BamD V192 chosen for disulfide engineering are highlighted in green.

(C) Effect of a BamD mutation in its interaction with BamD. Western blots of input (I), flow through (FT), wash (W), and elution (E) fractions from an Ni-NTA purification of *E. coli* JCM166 cells expressing wild-type His-tagged ecBamA and ecBamD wild-type (BamD WT) or an A193W mutant (BamD A193W), probed with anti-BamA (αBamA) or anti-BamD (αBamD) antibodies. BamA interacts with endogenous BamD (En) and plasmid-encoded (Pl) BamD WT but not with plasmid-encoded BamD A193W. Plasmid-encoded BamD has a 2.1 kDa C-terminal tail to distinguish it from endogenous BamD.

(D) Interface probing by disulfide crosslinking. Western blots of input (Input) and elution (Elut.) fractions from an Ni-NTA purification of solubilized *coli* JCM290 cells expressing His-tagged ecBamA G374C and ecBamD V192C (X lanes), which are close in the BamA-BamD interface (B, green); or expressing BamA G374C and a control mutation in BamD S122C (C lanes), which is remote from the interface. SDS-PAGE was run with (+) or without (−) DTT and western blotted with anti-BamA (αBamA) or anti-BamD (αBamD) antibodies. Only cells expressing ecBamA G374C and ecBamD V192C (X lanes) display disulfide crosslinked BamA-BamD. See also Figures S1 and S2.

survive the in vitro assays, the data indicate that BamA E373 and BamD R197 stabilize the interface, providing initial validation of the interface observed in the crystallographic model.

Two complementary approaches were utilized to further validate the observed interface. First, a residue in ecBamD with a small side chain packed at the interface was identified (ecBamD A193), mutated to tryptophan in the full-length protein, and tested for its ability to interact with full-length BamA in vivo. The *E. coli* strain JCM166 developed by Wu et al. (2005) has the *bamA* gene under the control of an arabinose promoter and can thus be depleted of endogenous BamA by growth in fucose or glucose. As BamA is essential, these cells die after a few generations when grown in glucose. It was previously shown, however, that an N-terminally His-tagged form of BamA expressed from a constitutive promoter in the low copy number plasmid pZS21 can complement this phenotype, replacing the endogenous BamA with plasmid-borne, His-tagged BamA (Kim et al., 2007). Furthermore, His-tagged BamA assembles into functional BAM complexes and can thus be used for co-purification of interacting subunits (Kim et al., 2007). This plasmid was modified to incorporate a copy of the *bamD* gene downstream of *bamA* such that a polycistronic mRNA could drive expression of His-tagged BamA and BamD to be tested. To distinguish endogenous BamD from plasmid-borne BamD, the plasmid *bamD* gene was modified to encode 17 additional amino acids at the C terminus. Plasmid-borne BamD is thus 2.1 kDa bigger and can be distinguished from endogenous BamD in SDS-PAGE (Figure S2). This plasmid was used to transform *E. coli* JCM166. The cells were then grown in glucose to deplete them of endogenous BamA, solubilized with BugBuster and subjected to Ni-NTA purification followed by western blotting. As shown in Figure 2C, when BamD wild-type is expressed from the pZS21 plasmid together with His-tagged BamA, eluates (E) from Ni-NTA show that His-tagged BamA is able to co-purify with both endogenous (En) and plasmid-borne (Pl) BamD. However, when the plasmid encoded His-tagged BamA and BamD A193W, only endogenous BamD co-purified with BamA, consistent with the A193W mutation impairing BamA-BamD binding as predicted by the crystal structure.

In a second complementary approach, the BamA-BamD interface was probed using disulfide crosslinking. *E. coli* BamA and BamD are devoid of reactive cysteines. The single cysteine present in wild-type BamD is at its N terminus and thus lipidated. Whereas two cysteines are present in wild-type BamA, they reside in the β-barrel domain, face the outside of the cell, and are engaged in a disulfide bond (Albrecht et al., 2014). Therefore, single cysteines were introduced in BamA and BamD such that, according to the crystal structure, they could form an inter-subunit disulfide bond. The ecBamA-BamD model was analyzed with the server Disulfide by Design (Craig and Dombkowski, 2013), which identified ecBamA G374 and ecBamD V192 as residues that, when mutated to cysteine, would have distances and orientations compatible with inter-subunit disulfide bond formation according to the crystal structure. These mutations were incorporated into the pZS21 plasmid described above encoding His-tagged BamA(G374C) and BamD(V192C) to test for disulfide bond formation in the full-length proteins in vivo. As a control, His-tagged BamA(G374C) was also expressed together with BamD(S122C), which introduced a cysteine at a remote position from BamA(G374C) and, according to the crystal structure, would not be expected to form a disulfide. JCM290 *E. coli* cells, analogous to JCM166, have the endogenous *bamD* gene under

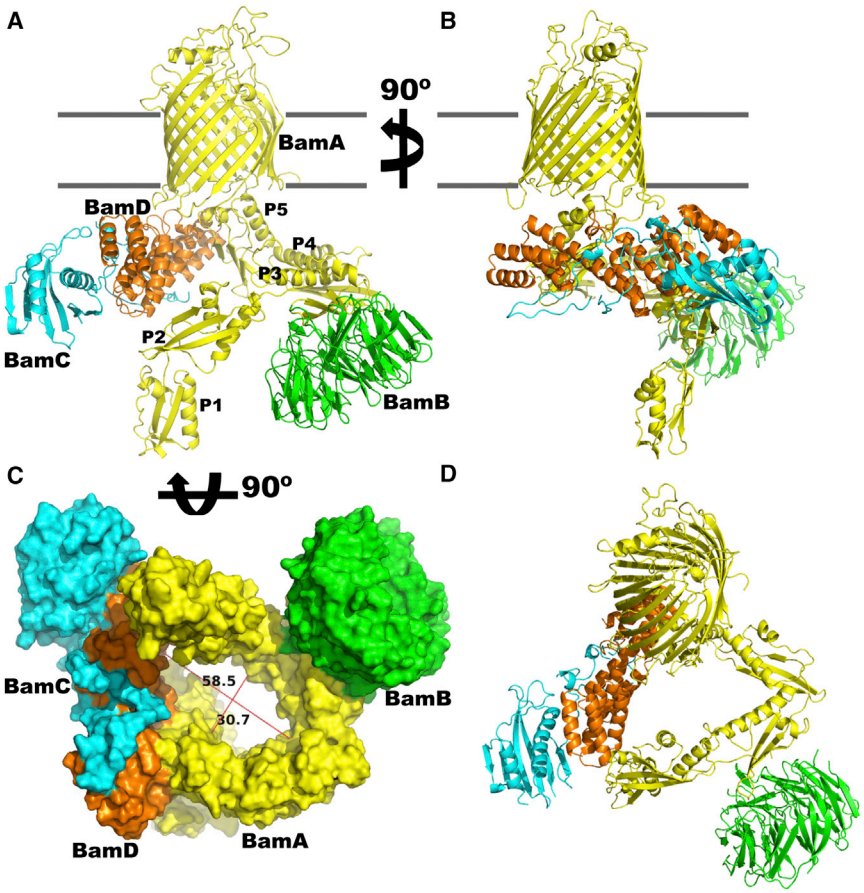

Figure 3. Model of the Core BamABCD Complex

(A) Cartoon representation of a BAM complex containing BamA (yellow), BamB (green), BamD (orange), and the N-terminal domains of BamC (cyan). The view is parallel to the membrane plane where the β-barrel domain of BamA is embedded. The POTRA domains 2–5 (P2–P5) and BamD form a periplasmic ring. POTRA1 extends below the ring, whereas BamB and BamC are arranged in the periphery.

(B) View of (A) rotated 90° around a right-handed y axis. The long axis of BamD (orange) is parallel to the membrane.

(C) Space-filling representation of the complex rotated approximately 90° around the x axis such that the view is from the periplasmic side and normal to the membrane. The periplasmic ring defines an elongated cavity approximately 30 × 60 Å in diameter.

(D) Cartoon representation of the complex viewed at a 45° angle from the membrane plane from the outside of the cell without any membrane representation to show the periplasmic ring.

the arabinose promoter (Wu et al., 2005). JCM290 cells were transformed with these plasmids and grown in glucose to deplete them of endogenous BamD. Cultures grown to late log phase were then harvested and immediately treated with 4 mM *N*-ethyl-maleimide (NEM) to quench disulfide bond formation. After solubilization with BugBuster and Ni-NTA purification, inputs and elutions were analyzed by western blotting probed with antibodies against BamA and BamD. As shown in Figure 2D, cells expressing His-tagged BamA(G374C) and BamD(V192C) (labeled X in Figure 2D) display a band with molecular weight higher than BamA, which reacts with both BamA and BamD antibodies when the samples are run in the absence of the reducing agent DTT. This high molecular weight band (highlighted with a double arrow) disappears when the samples are treated with DTT, indicating that the band corresponds to disulfide-linked BamA-BamD. Conversely, cells expressing the control proteins His-tagged BamA(G374C) and BamD(S122C) (labeled C in Figure 2D) do not display the high molecular weight band, as expected based on their distant locations in the crystal structure. These results strongly support the conclusion that the interface observed in the crystal structure captures the native interface present in the full-length proteins.

Architecture of the BAM Core Complex

BamAB and BamCDE subcomplexes can be isolated and brought together to form a functional BAM holocomplex (Hagan and Kahne, 2011; Hagan et al., 2010). Availability of the structures of *Neisseria gonorrhoeae* BamA containing both its membrane-embedded β-barrel and the periplasmic POTRA domains (Noinaj et al., 2013), as well as that of the *E. coli* BamA-BamB fusion, has allowed modeling of the BamAB subcomplex (Jansen et al., 2015). The crystal structure of BamD in complex with the N-terminal domains of BamC (Kim et al., 2011) as well as the structure of BamA-BamD presented here can now be used to gain insight into the architecture of a more complete BAM complex that is only missing the small BamE subunit and the C-terminal domain of BamC. The structure of full-length *Neisseria gonorrhoeae* BamA was used as a scaffold onto which the high-resolution structure of the ecBamA β-barrel was superimposed. The structure of ecBamA POTRA5-BamD presented here was then superimposed onto POTRA5. Similarly, the structure of ecBamA POTRA3-BamB (Jansen et al., 2015) was superimposed onto POTRA3 and the structures of ecBamA POTRA1-2 and POTRA4 were individually superimposed. Finally, the structures of the N-terminal domains of BamC were added to the model by superimposing BamD in the BamCD complex (Kim et al., 2011). This produced a model of *E. coli* BAM with no clashes. The model was then subjected to a round energy minimization using the Pareto-optimal refinement method implemented in Rosetta (Nivon et al., 2013). This approach reduces model strain while restraining the minimization to maintain good agreement with the experimentally derived input coordinates. The resulting model provides a first glimpse at the architecture of a BamABCD complex (Figure 3).

DISCUSSION

Outer membrane biogenesis is an essential process for diderm (also known as Gram-negative) bacteria. Its integral membrane

proteins have a characteristic β-barrel structure and their folding and insertion are complex processes requiring the concerted action of an inner membrane translocon, periplasmic chaperones, and the multiprotein BAM in the outer membrane (Hagan et al., 2011). BamA is clearly the central component of BAM and it has been shown that BamA by itself is capable of accelerating OMP folding into liposomes made of synthetic lipids (Gessmann et al., 2014; Patel and Kleinschmidt, 2013). However, its full in vivo function requires its assembly into a complex with the lipoproteins BamBCDE. BamD is the only essential lipoprotein component of BAM and it has recently been proposed to participate in recognition of nascent OMPs (Hagan et al., 2015). As both the C terminus of the periplasmic domain of BamA and the N terminus of BamD are topologically close to the membrane, we followed the strategy of joining these two ends with a flexible linker resulting in a fusion for structure determination that could capture the interaction between the two essential components of BAM. The fusion of *R. marinus* BamA POTRA4-5 and BamD yielded crystals, which were used to determine the structure and refine it to 2.0-Å resolution.

Whereas several interfaces between BamA and BamD are observed in the $P2_1$ lattice of the crystals, the interface depicted in Figure 1 is the largest, burying approximately 650 $Å^2$ of surface area. Nevertheless, it was important to validate that the observed interface was physiologically relevant and not a crystallographic artifact of the fusion protein. Excellent superposition of the high-resolution crystal structures of *E. coli* POTRA5 and BamD on the *Rhodothermus* fusion protein suggested that the interface would be structurally conserved. However, *E. coli* and *Rhodothermus* BAM subunits share approximately 20% sequence identity and many of the interface residues appear to have co-varied, making functional testing of the observed interface in *E. coli* difficult. We thus improved the superimposed model using the high-resolution comparative modeling protocol implemented in the Rosetta suite, RosettaCM (Song et al., 2013). In the resulting model, ecBamA E373 and ecBamD R197 form a salt bridge that would stabilize the interface. It has previously been reported that an ecBamA E373K mutation results in loss of BamD binding and is thus lethal to cells. The lethal phenotype can be rescued by an ecBamD R197L mutation. These results are fully consistent with the model interface and provide initial validation that the BamA-BamD crystal structure presented here is physiologically relevant.

In the rmBamA-BamD structure, the POTRA5 domain of rmBamA binds in a groove formed by the BamD TPR4 and the loop connecting the two helices of TPR3. This loop provides several stabilizing interactions (Figure 1B). However, this loop is extended and conformationally labile in ecBamD as demonstrated by its absence from the high-resolution structures of isolated ecBamD (Albrecht and Zeth, 2011; Dong et al., 2012). While it was possible to build this loop into the model of the ecBamD-BamC structure (Kim et al., 2011) (Figure S1), its conformation is stabilized by a lattice contact and thus may not represent a highly populated conformation without the lattice constrains. This conformational lability was also captured in the RosettaCM models (data not shown), making it difficult to design point mutations to validate the crystallographic model by disrupting the ecBamA-BamD interface beyond the BamA E373K mutation already described. We thus took the approach of identifying a small side chain packed in a structurally well-conserved part of the interface and replacing it with the bulky tryptophan residue to disrupt the interface by steric hindrance. This strategy is routinely used to disrupt helix packing interactions (Santiago et al., 2004; Sharp et al., 1995). As shown in Figure 2C, ecBamD A193W fails to co-purify with His-tagged ecBamA whereas wild-type proteins interact normally, consistent with A193 being at the interface between BamA and BamD as shown in the crystallographic model.

Whereas validation of the protein-protein interfaces by mutations that disrupt the interaction is a valuable approach, disulfide engineering is a powerful complementary method that provides a positive signal (disulfide formation) if the proteins are arranged as defined in the crystal structure. Analysis of the ecBamA-BamD model indicated that mutation of BamA G374 and BamD V192 to cysteine would be favorably positioned to form inter-subunit disulfide bonds. Indeed, expression of His-tagged BamA (G374C) and BamD (V192C) yielded a disulfide cross-linked band formed efficiently in vivo without addition of an external oxidizing agent. This strongly suggests that BamA and BamD interact in vivo as depicted in the crystallographic model.

Taken together, the mutagenesis and disulfide crosslinking experiments indicate that the crystal structure presented here represents the native, physiologically relevant interface between BamA and BamD.

The structures of full-length BamA (Noinaj et al., 2013), a BamA-BamB fusion (Jansen et al., 2015), BamD in complex with the N-terminal domains of BamC (Kim et al., 2011), and the BamA-BamD fusion presented here, were used to build a model of the *E. coli* BamABCD complex (Figure 3). In the model, BamA POTRA2-5 and BamD form an elongated periplasmic ring with its central axis perpendicular to the membrane plane and a central cavity approximately 30- by 60-Å wide (Figure 3C). The BamA POTRA1 extends below the ring while the lipoproteins BamB and BamC are arranged in the ring periphery. Nascent OMPs have been proposed to bind the S2 strands of BamA POTRA domains thereby extending their β-sheet in a process called β-augmentation. Recently, BamD has also been implicated in direct interaction with substrate OMPs (Hagan et al., 2015). In the model, the S2 strands of POTRA3-5 are exposed to the central ring cavity that is also lined by BamD (Figure 3D). It is therefore tempting to propose that nascent OMPs may be accommodated in the elongated ring cavity adjacent to the membrane as a prelude to membrane insertion and folding. Whereas the mechanisms of OMP insertion and folding are not known, current proposals include insertion into BamA-induced lipid defects in the vicinity of the BamA β-barrel (Danoff and Fleming, 2015; Fleming, 2015; Gessmann et al., 2014; Noinaj et al., 2013) as well as insertion of β-hairpins from nascent OMPs between the first and last strands of the BamA β-barrel whereby nascent β-barrels would bud from the BamA β-barrel (Noinaj et al., 2013, 2014, 2015). Both mechanisms would be facilitated by binding of nascent OMPs in a membrane-adjacent cavity such as the one described in the BamABCD model.

Analysis of the BamA crystal structures has identified significant flexibility in the connection between POTRA5 and the β-barrel (Albrecht et al., 2014; Noinaj et al., 2014; Noinaj et al., 2015), which would allow the entire periplasmic domain of BamA to sample many different conformations, from extended and

perpendicular to the membrane to an arrangement in which all POTRA domains are close to the membrane. However, complexation with BamCD as shown in the model would restrict the possible BamA conformations. BamD binds POTRA5 such that the long axis of BamD would be parallel and adjacent to the membrane plane (Figure 3B). With this arrangement, the membrane-embedded BamA β-barrel and the periplasmic ring could rotate with respect to one another such that their central axes are collinear or offset. However, tilting of the periplasmic ring with respect to the membrane would be more restricted by interaction of the BamCD subunits with the membrane. While not present in the current model, BamE is part of the BamCDE subcomplex and has been shown to interact with lipids (Knowles et al., 2011), which may further restrict the mobility of the periplasmic ring of BAM in vivo.

Of the non-essential BAM lipoproteins (BamBCE), BamB appears to be the most important as judged by the severity of the phenotypes associated with their *null* mutations (Sklar et al., 2007a; Wu et al., 2005). Based on analysis of its high-resolution structure, BamB has been proposed to interact directly with nascent OMPs (Gatsos et al., 2008; Heuck et al., 2011). However, experimental testing of those proposals has been negative (Jansen et al., 2012). The non-essential lipoprotein may instead have a role in modulating the conformations of the essential subunits BamA and BamD. The location of BamB and BamC in the periphery of the periplasmic ring of BAM is consistent with this idea. BamB binds the POTRA3 of BamA and is positioned to also interact with POTRA2 (Jansen et al., 2015). It is thus ideally positioned to modulate flexibility of the hinge that links POTRA2 and POTRA3. Such flexibility could open the periplasmic ring laterally or plug the bottom of the ring depending on the orientation adopted by the POTRA1-2 subdomain. This model provides a first glimpse at the architecture of the BamABCD model as a platform to develop mechanistic hypotheses of β-barrel OMP insertion and folding.

EXPERIMENTAL PROCEDURES

Cloning expression and purification of BamA (POTRA4-5)-BamD is detailed in the Supplemental Experimental Procedures.

Protein Crystallization and Structure Determination

Crystallization screening of the BamA (POTRA4-5)-BamD fusion protein was carried out at 16°C using the sitting drop vapor diffusion method. Initial crystallizing conditions were refined using the hanging drop method to 10% PEG-3000, 15% 2-propanol, and 0.1 M HEPES (pH 5.6), combining 1.5 μl of mother liquor and 1.5 μl of 12 mg/ml protein at 25°C. Crystals formed after a week as thin plates. For data collection, crystals were harvested and cryoprotected in mother liquor supplemented with 20% ethylene glycol before being flash frozen in liquid nitrogen. An X-ray diffraction dataset to 2.0 Å resolution was collected at beamline 5.0.2 of the Advanced Light Source of the Lawrence Berkeley National Laboratory. After reduction using HKL2000 (Otwinowski and Minor, 1997), the data were used to determine the crystal structure with molecular replacement methods using the PHENIX software suite (Adams et al., 2010). The structure of *R. marinus* BamD (Sandoval et al., 2011) was divided into N- and C-terminal subdomains and used as sequential search models resulting in clear rotation and translation search solutions. The structure of *E. coli* BamA POTRA4-5 (Gatzeva-Topalova et al., 2010) was then used as a search model after converting all residues to alanine. This also produced a clear rotation-translation solution. Using PHENIX, the model was then subjected to a round of rigid body refinement of four groups: BamD N terminus, BamD C terminus, BamA POTRA4, and BamA POTRA5. A few sections of the BamA POTRA domains that did not agree with the electron density were removed. Several iterations of positional and B-factor refinement in PHENIX interspersed with manual rebuilding in Coot (Emsley and Cowtan, 2004) resulted in a final model with excellent geometry and no chain breaks. Data collection and refinement statistics are summarized in Table 1.

Co-purification, Disulfide Crosslinking, and Western Blotting

E. coli strain JCM166 and the pZS21 plasmid encoding *E. coli* BamA were a kind gift from Dr. Thomas Silhavy (Princeton University) (Wu et al., 2005). The pZS21 plasmid was modified to incorporate a canonical Shine-Delgarno sequence upstream of *bamA* and a His-tag between the signal sequence and the first POTRA domain of BamA. A restriction site downstream of *bamA* was then used to ligate the gene for full-length *E. coli* BamD PCR amplified from genomic DNA. The C-terminal primer incorporated a C-terminal tail encoding amino acids (DYKDDDDKYPYDVPDYA) increasing the size of plasmid-encoded ecBamD by 2.1 kDa to facilitate its separation from endogenous ecBamD in western blotting experiments. This resulted in plasmid pMS1102. The quick-change mutagenesis protocol was then utilized to introduce a BamD A193W mutation in this plasmid resulting in pMS 1303 (His-BamA, BamDA193W). Sequential rounds of mutagenesis were used to introduce cysteine residues in BamA and BamD to generate plasmids pMS1308 (His-BamA G374C, BamD V192C) as well as pMS1310 (His-BamA G374C, BamD S122C).

For co-purification and western blotting, *E. coli* JCM 166 (BamA depletion cells) were transformed with pMS1102 or pMS1303 (BamD A193W) and plated on LB (lysogeny broth, Miller)/Kan 0.1% arabinose plates. A single colony was used to inoculate a 5-ml culture in LB/Kan 0.1% arabinose that was incubated at 37°C overnight. Cells were spun down and washed twice with fresh LB and used to inoculate a 5-ml culture of LB/Kan 0.1% glucose (glucose or fucose can be used to shut down expression of the *bamA* gene for endogenous BamA depletion). Cultures were grown at 37°C to an OD_{600} ~0.6 and diluted down to OD_{600} of 0.05 in LB/Kan 0.1% glucose to keep them growing in log phase. This was repeated four times in total (until control cultures without a plasmid copy of *bamA* stop growing, data not shown) to deplete the cells of endogenous BamA, and the final 5-ml culture was used to inoculate a 200-ml culture of LB/Kan 0.1% glucose. This was grown to OD_{600} of 0.6, and the cells harvested by centrifugation in 100-ml aliquots. Cell weight was determined and the cells solubilized by adding BugBuster (Merck Millipore) at a ratio of 5 ml/g of cells (~1.5 ml) supplemented with Halt Protease & Phosphatase Inhibitor cocktail (Thermo Scientific), 100 μg/ml lysozyme, and 2 μl of Benzonase (Novagen). After incubation for 1 hr in a tube rocker at room temperature, the lysate was spun down for 20 min at 21,000 × *g* to remove cell debris and the pH adjusted to 8.0. The clarified lysate was loaded on to 250 μl of Ni-NTA (Qiagen) pre-equilibrated with buffer D (10 mM Tris [pH 8.0], 150 mM NaCl, 0.5% Triton X-100) and incubated at room temperature for 45 min with periodic agitation. The Ni-NTA beads were packed in a column, washed with 5 column volumes of buffer D, and eluted in 100-μl fractions of buffer E (buffer D and 500 mM imidazole). The second elution fraction, along with the last 250-μl wash fraction, and the input were mixed with SDS loading dye, boiled for 5 min, and run on 4%–20% SDS-PAGE (GenScript). Gels were transferred to polyvinylidene fluoride membranes (EMD Millipore) and probed with BamA (1:20,000 dilution) or BamD (1:5,000 dilution) polyclonal antibodies raised against these proteins (Cocalico Biologicals). Secondary goat anti-rabbit HRP conjugated antibodies (Pierce) (1:25,000 dilution) and Western Lightning ECL Pro HRP substrate (PerkinElmer) were used for detection.

For disulfide crosslinking experiments, JCM290 cells were transformed with pMS1308 (His-BamA G374C, BamD V192C) or pMS1310 (His-BamA G374C, BamD S122C) and treated as described above for co-purification experiments with the following modifications: (1) cells were solubilized with BugBuster containing 100 μg/ml lysozyme, 1× Halt! Protease Inhibitor (Thermo Fisher), and 1 μl (25 U/μL) of Benzonase (Novagen) nuclease as well as 4 mM NEM to block any free cysteines and quench disulfide formation during processing. (2) 125 μl of Ni-NTA was used to purify His-tagged BamA complexes; and (3) the SDS loading dye was supplemented with NEM to a final concentration of 10 mM to prevent disulfide bond formation during sample boiling. The western blots were carried out described above.

ACCESSION NUMBERS

Atomic coordinates and structure factor amplitudes have been deposited in the PDB under PDB: 5EFR.

SUPPLEMENTAL INFORMATION

Supplemental Information includes Supplemental Experimental Procedures, two figures, and the *E.coli* BamABCD model and can be found with this article online at http://dx.doi.org/10.1016/j.str.2015.10.030.

AUTHOR CONTRIBUTIONS

H.T.B., A.H.H, S.I.M., and M.C.S designed and conducted the experiments. H.T.B., A.H.H, S.I.M., and M.C.S analyzed the results. M.S. wrote the manuscript with assistance from H.B., A.H., and S.M.

ACKNOWLEDGMENTS

We thank Dr. David B. McKay for support at the X-ray crystallography facility of the University of Colorado Boulder. This research was supported in part by NIH grant R01 AI080709 to M.C.S. Part of the work presented in this manuscript was carried out at the Advanced Light Source, which is supported by the Director, Office of Science, Office of Basic Energy Sciences, of the U.S. Department of Energy under Contract No. DE-AC02-05CH11231.

Received: September 23, 2015
Revised: October 25, 2015
Accepted: October 27, 2015
Published: December 31, 2015

REFERENCES

Adams, P.D., Afonine, P.V., Bunkoczi, G., Chen, V.B., Davis, I.W., Echols, N., Headd, J.J., Hung, L.W., Kapral, G.J., Grosse-Kunstleve, R.W., et al. (2010). PHENIX: a comprehensive Python-based system for macromolecular structure solution. Acta Crystallogr. D Biol. Crystallogr. *66*, 213–221.

Albrecht, R., and Zeth, K. (2011). Structural basis of outer membrane protein biogenesis in bacteria. J. Biol. Chem. *286*, 27792–27803.

Albrecht, R., Schutz, M., Oberhettinger, P., Faulstich, M., Bermejo, I., Rudel, T., Diederichs, K., and Zeth, K. (2014). Structure of BamA, an essential factor in outer membrane protein biogenesis. Acta Crystallogr. D Biol. Crystallogr. *70*, 1779–1789.

Allan, R.K., and Ratajczak, T. (2010). Versatile TPR domains accommodate different modes of target protein recognition and function. Cell Stress Chaperones *16*, 353–367.

Bos, M.P., Tefsen, B., Geurtsen, J., and Tommassen, J. (2004). Identification of an outer membrane protein required for the transport of lipopolysaccharide to the bacterial cell surface. Proc. Natl. Acad. Sci. USA *101*, 9417–9422.

Craig, D.B., and Dombkowski, A.A. (2013). Disulfide by Design 2.0: a web-based tool for disulfide engineering in proteins. BMC Bioinformatics *14*, 346.

Danoff, E.J., and Fleming, K.G. (2015). Membrane defects accelerate outer membrane beta-barrel protein folding. Biochemistry *54*, 97–99.

Dong, C., Hou, H.F., Yang, X., Shen, Y.Q., and Dong, Y.H. (2012). Structure of Escherichia coli BamD and its functional implications in outer membrane protein assembly. Acta Crystallogr. D Biol. Crystallogr. *68*, 95–101.

Emsley, P., and Cowtan, K. (2004). Coot: model-building tools for molecular graphics. Acta Crystallogr. D Biol. Crystallogr. *60*, 2126–2132.

Endo, T., Kawano, S., and Yamano, K. (2011). BamE structure: the assembly of beta-barrel proteins in the outer membranes of bacteria and mitochondria. EMBO Rep. *12*, 94–95.

Fleming, K.G. (2015). A combined kinetic push and thermodynamic pull as driving forces for outer membrane protein sorting and folding in bacteria. Philos. Trans. R. Soc. Lond. B Biol. Sci. *370*.

Gatsos, X., Perry, A.J., Anwari, K., Dolezal, P., Wolynec, P.P., Likic, V.A., Purcell, A.W., Buchanan, S.K., and Lithgow, T. (2008). Protein secretion and outer membrane assembly in Alphaproteobacteria. FEMS Microbiol. Rev. *32*, 995–1009.

Gatzeva-Topalova, P.Z., Walton, T.A., and Sousa, M.C. (2008). Crystal structure of YaeT: conformational flexibility and substrate recognition. Structure *16*, 1873–1881.

Gatzeva-Topalova, P.Z., Warner, L.R., Pardi, A., and Sousa, M.C. (2010). Structure and flexibility of the complete periplasmic domain of BamA: the protein insertion machine of the outer membrane. Structure *18*, 1492–1501.

Gentle, I., Gabriel, K., Beech, P., Waller, R., and Lithgow, T. (2004). The Omp85 family of proteins is essential for outer membrane biogenesis in mitochondria and bacteria. J. Cell Biol. *164*, 19–24.

Gessmann, D., Chung, Y.H., Danoff, E.J., Plummer, A.M., Sandlin, C.W., Zaccai, N.R., and Fleming, K.G. (2014). Outer membrane beta-barrel protein folding is physically controlled by periplasmic lipid head groups and BamA. Proc. Natl. Acad. Sci. USA *111*, 5878–5883.

Hagan, C.L., and Kahne, D. (2011). The reconstituted Escherichia coli Bam complex catalyzes multiple rounds of beta-barrel assembly. Biochemistry *50*, 7444–7446.

Hagan, C.L., Kim, S., and Kahne, D. (2010). Reconstitution of outer membrane protein assembly from purified components. Science *328*, 890–892.

Hagan, C.L., Silhavy, T.J., and Kahne, D. (2011). beta-Barrel membrane protein assembly by the Bam complex. Annu. Rev. Biochem. *80*, 189–210.

Hagan, C.L., Wzorek, J.S., and Kahne, D. (2015). Inhibition of the beta-barrel assembly machine by a peptide that binds BamD. Proc. Natl. Acad. Sci. USA *112*, 2011–2016.

Heinz, E., and Lithgow, T. (2014). A comprehensive analysis of the Omp85/TpsB protein superfamily structural diversity, taxonomic occurrence, and evolution. Front Microbiol. *5*, 370.

Heuck, A., Schleiffer, A., and Clausen, T. (2011). Augmenting beta-augmentation: structural basis of how BamB binds BamA and may support folding of outer membrane proteins. J. Mol. Biol. *406*, 659–666.

Hsu, S.C., and Inoue, K. (2009). Two evolutionarily conserved essential beta-barrel proteins in the chloroplast outer envelope membrane. Biosci. Trends *3*, 168–178.

Jansen, K.B., Baker, S.L., and Sousa, M.C. (2012). Crystal structure of BamB from Pseudomonas aeruginosa and functional evaluation of its conserved structural features. PLoS One *7*, e49749.

Jansen, K.B., Baker, S.L., and Sousa, M.C. (2015). Crystal structure of BamB bound to a periplasmic domain fragment of BamA, the central component of the beta-barrel assembly machine. J. Biol. Chem. *290*, 2126–2136.

Kim, K.H., and Paetzel, M. (2011). Crystal structure of Escherichia coli BamB, a lipoprotein component of the beta-barrel assembly machinery complex. J. Mol. Biol. *406*, 667–678.

Kim, S., Malinverni, J.C., Sliz, P., Silhavy, T.J., Harrison, S.C., and Kahne, D. (2007). Structure and function of an essential component of the outer membrane protein assembly machine. Science *317*, 961–964.

Kim, K.H., Aulakh, S., and Paetzel, M. (2011). Crystal structure of beta-barrel assembly machinery BamCD protein complex. J. Biol. Chem. *286*, 39116–39121.

Knowles, T.J., Browning, D.F., Jeeves, M., Maderbocus, R., Rajesh, S., Sridhar, P., Manoli, E., Emery, D., Sommer, U., Spencer, A., et al. (2011). Structure and function of BamE within the outer membrane and the beta-barrel assembly machine. EMBO Rep. *12*, 123–128.

Krissinel, E., and Henrick, K. (2007). Inference of macromolecular assemblies from crystalline state. J. Mol. Biol. *372*, 774–797.

Lyu, Z.X., and Zhao, X.S. (2015). Periplasmic quality control in biogenesis of outer membrane proteins. Biochem. Soc. Trans. *43*, 133–138.

Nivon, L.G., Moretti, R., and Baker, D. (2013). A Pareto-optimal refinement method for protein design scaffolds. PLoS One *8*, e59004.

Noinaj, N., Fairman, J.W., and Buchanan, S.K. (2011). The crystal structure of BamB suggests interactions with BamA and its role within the BAM complex. J. Mol. Biol. *407*, 248–260.

Noinaj, N., Kuszak, A.J., Gumbart, J.C., Lukacik, P., Chang, H., Easley, N.C., Lithgow, T., and Buchanan, S.K. (2013). Structural insight into the biogenesis of beta-barrel membrane proteins. Nature *501*, 385–390.

Noinaj, N., Kuszak, A.J., Balusek, C., Gumbart, J.C., and Buchanan, S.K. (2014). Lateral opening and exit pore formation are required for BamA function. Structure *22*, 1055–1062.

Noinaj, N., Rollauer, S.E., and Buchanan, S.K. (2015). The beta-barrel membrane protein insertase machinery from Gram-negative bacteria. Curr. Opin. Struct. Biol. *31*, 35–42.

Otwinowski, Z., and Minor, W. (1997). Processing of X-ray diffraction data collected in oscillation mode. Methods Enzymol. *276*, 307–326.

Patel, G.J., and Kleinschmidt, J.H. (2013). The lipid bilayer-inserted membrane protein BamA of Escherichia coli facilitates insertion and folding of outer membrane protein A from its complex with Skp. Biochemistry *52*, 3974–3986.

Ricci, D.P., Hagan, C.L., Kahne, D., and Silhavy, T.J. (2012). Activation of the Escherichia coli beta-barrel assembly machine (Bam) is required for essential components to interact properly with substrate. Proc. Natl. Acad. Sci. USA *109*, 3487–3491.

Ruiz, N., Falcone, B., Kahne, D., and Silhavy, T.J. (2005). Chemical conditionality: a genetic strategy to probe organelle assembly. Cell *121*, 307–317.

Sandoval, C.M., Baker, S.L., Jansen, K., Metzner, S.I., and Sousa, M.C. (2011). Crystal structure of BamD: an essential component of the β-Barrel assembly machinery of gram-negative bacteria. J. Mol. Biol. *409*, 348–357.

Santiago, J., Guzman, G.R., Torruellas, K., Rojas, L.V., and Lasalde-Dominicci, J.A. (2004). Tryptophan scanning mutagenesis in the TM3 domain of the *Torpedo californica* acetylcholine receptor beta subunit reveals an alpha-helical structure. Biochemistry *43*, 10064–10070.

Sharp, L.L., Zhou, J., and Blair, D.F. (1995). Tryptophan-scanning mutagenesis of MotB, an integral membrane protein essential for flagellar rotation in *Escherichia coli*. Biochemistry *34*, 9166–9171.

Sklar, J.G., Wu, T., Gronenberg, L.S., Malinverni, J.C., Kahne, D., and Silhavy, T.J. (2007a). Lipoprotein SmpA is a component of the YaeT complex that assembles outer membrane proteins in *Escherichia coli*. Proc. Natl. Acad. Sci. USA *104*, 6400–6405.

Sklar, J.G., Wu, T., Kahne, D., and Silhavy, T.J. (2007b). Defining the roles of the periplasmic chaperones SurA, Skp, and DegP in *Escherichia coli*. Genes Dev. *21*, 2473–2484.

Song, Y., DiMaio, F., Wang, R.Y., Kim, D., Miles, C., Brunette, T., Thompson, J., and Baker, D. (2013). High-resolution comparative modeling with RosettaCM. Structure *21*, 1735–1742.

Sutcliffe, I.C. (2010). A phylum level perspective on bacterial cell envelope architecture. Trends Microbiol. *18*, 464–470.

Volokhina, E.B., Grijpstra, J., Stork, M., Schilders, I., Tommassen, J., and Bos, M.P. (2011). Role of the periplasmic chaperones Skp, SurA, and DegQ in outer membrane protein biogenesis in *Neisseria meningitidis*. J. Bacteriol. *193*, 1612–1621.

Voulhoux, R., and Tommassen, J. (2004). Omp85, an evolutionarily conserved bacterial protein involved in outer-membrane-protein assembly. Res. Microbiol. *155*, 129–135.

Vuong, P., Bennion, D., Mantei, J., Frost, D., and Misra, R. (2008). Analysis of YfgL and YaeT interactions through bioinformatics, mutagenesis, and biochemistry. J. Bacteriol. *190*, 1507–1517.

Warner, L.R., Varga, K., Lange, O.F., Baker, S.L., Baker, D., Sousa, M.C., and Pardi, A. (2011). Structure of the BamC two-domain protein obtained by Rosetta with a limited NMR data set. J. Mol. Biol. *411*, 83–95.

Wu, T., Malinverni, J., Ruiz, N., Kim, S., Silhavy, T.J., and Kahne, D. (2005). Identification of a multicomponent complex required for outer membrane biogenesis in Escherichia coli. Cell *121*, 235–245.